Title: Maturational networks of fetal brain activity

Authors: Karolis VR[1,2,*], Fitzgibbon SP[2], Cordero-Grande L[3], Farahibozorg R[2], Price AN[1], Hughes EJ[1], Fetit AE[4,5], Kariakopoulou V[1], Pietsch, M[1], Rutherford MA[1], Rueckert D[4,6], Hajnal JV[1], Edwards AD[1,7], O'Muircheartaigh J[1,7,8], Duff EP[2,9,#] & Arichi T[1,7,10,#]

1. Centre for the Developing Brain, School of Biomedical Engineering and Imaging Sciences, King's College London, UK.
2. Wellcome Centre for Integrative Neuroimaging, FMRIB, Nuffield Department of Clinical Neurosciences, University of Oxford, UK.
3. Biomedical Image Technologies, ETSI Telecomunicación, Universidad Politécnica de Madrid & CIBER-BBN, Madrid, Spain
4. Biomedical Image Analysis Group, Department of Computing, Imperial College London, UK.
5. UKRI CDT in Artificial Intelligence for Healthcare, Department of Computing, Imperial College London, London, UK
6. Department of Medicine and Informatics, Technical University of Munich, Munich, Germany.
7. MRC Centre for Neurodevelopmental Disorders, King's College London, UK.
8. Department of Forensic and Neurodevelopmental Sciences, Institute of Psychiatry, Psychology & Neuroscience, King's College London, London SE5 8AF, UK.
9. Department of Brain Sciences, Faculty of Medicine, Imperial College London, UK.
10. Paediatric Neurosciences, Evelina London Children's Hospital, Guy's and St Thomas' NHS Foundation Trust, United Kingdom.

* - corresponding author, slava.karolis@kcl.ac.uk

\# - equally contributing last authors

ABSTRACT

The human fetal period is associated with a rapid emergence of body organ functions and systems, including establishment of the functional brain connectome. In order to characterise developmental features of in-utero functional activity, we introduce a novel perspective on resting-state functional networks, which we call "maturational networks", or "matnets". The key feature of this framework is that it incorporates age-related changes in connectivity into network estimation, thereby characterising functional networks as an emerging property of the brain. We find that fetal matnets reveal several spatially distributed patterns of connections with remarkable anatomical specificity. The framework also enables construction of a whole-brain view of maturational relationships across the early brain's functional organisation, which we term the "maturational connectome". We find that the fetal maturational connectome is composed of several groups of maturational networks, among which two groups which are associated with active environmental interaction through perceptual and motor-planning mechanisms, assume a central role.

INTRODUCTION

Does a 'thing' possess invariant properties, its 'being', or is the essence of its existence in its change and thus in its 'becoming'? This ancient intellectual dilemma, conceived by an early Greek philosopher Heraclitus, has been entwined in the centuries-long evolution of human knowledge[1,2]. At its core, it reflects a fundamental problem of selecting an appropriate representational framework for a phenomenon at study while offering a choice between two extreme alternatives. On the one hand, a description of invariant (canonical, typical) characteristics serves a purpose of giving a phenomenon a concrete definition and thus differentiating it from other things. On the other hand, representations that characterise a phenomenon as a process are more fitting if the phenomenon constitutes a sequence of superseding transient states with ill-defined invariant characteristics.

The notion of functional networks in the fetal brain is a case in point for the latter. Evidence from animal models suggests that intrinsically generated neural activity in the prenatal brain first begins with local direct propagation before progressing to larger bursts of spontaneous activity which help to establish local circuitry[3]. At around 26 weeks of gestation, as suggested by the ex-utero resting-state functional MRI (fMRI) studies of very preterm infants[4], spatially distinct networks emerge, showing local patterns of connectivity with a lack of long range interhemispheric or dorsocaudal connections. Towards term equivalent age, the networks evolve into a set of spatially distributed (multi-nodal) co-activation patterns [5,6], reflecting a generic drift of organic functions towards forming increasingly complex systems[7]. Such rapid developmental changes mean that functional networks in the prenatal period possess the attributes of an intrinsically non-static entity, a characteristic example of Heraclitian "becoming".

Previous research has demonstrated that, despite enormous technological challenges, functional connectivity in utero can now be studied using resting-state fMRI [8-10] . This opens up an opportunity for the use of standard approaches to group-level fMRI network analyses[11] such as group independent component analysis (group-ICA) [12-14]. The latter describes functional networks as a collection of spatial maps[15], each of them charting areas linked together by the strength of covariation between the timecourses of their fluctuating intrinsic activity. However, utility of this method for application with fetal data remains an open question, both conceptually and when considering the unique signal properties of the data acquired in utero. Conceptually, an assumption embedded into this method is that a group-level spatial map characterises a canonical form of a functional network with respect to its individual manifestations, thereby downgrading developmental changes in its spatial layout to the status of non-systematic, and likely underestimated [16], inter-subject variability. As a result, coherent developmental features that are fundamental to both a definition and understanding of the neuroscientific basis of functional networks in utero may be lost using the standard approach.

In this paper we introduce a novel perspective on resting-state functional networks in utero, which we call "maturational networks", or matnets for conciseness. The key feature of this framework is that it incorporates age-related changes in connectivity into network estimation, thereby characterising functional networks as an emerging property of the brain. At its core, it builds on Flechsig's idea[17], that functionally related areas mature together. In

contrast to the standard analytical approach of ICA, which utilises correlational structure to factorise networks, our approach leverages age-related changes in correlations in order to characterise maturational modes of variation in the data. The utility of this approach is demonstrated in in-utero fMRI data acquired as part of the developing Human Connectome Project (dHCP)[18,19], an open science initiative aiming to map brain connectivity across the perinatal period. The data, of unprecedented sample size, quality and length, were reconstructed and preprocessed using cutting-edge methodologies[20-22]. We show that our novel approach overcomes the inherent limitations of fMRI data acquired in-utero for characterising mid- and long-distance connectivity, and for inference about the developmental trajectory of the fetal functional connectome. Moreover, it enables factorisation of spatial patterns that fit better the concept of resting-state network as we understand it from the studies of more mature brains, that is, as a spatially distributed configuration encompassing non-adjacent brain areas[23,24]. Finally, we show that maturational networks lead to a new perspective on the macro-scale developmental relationships in the human brain, the "maturational connectome".

RESULTS

12.8 mins of resting state fMRI data was acquired from 144 fetuses with an age range between 25 and 38 gestation weeks (Supplementary Figure 1) on a 3T Philips Achieva system[25] as part of the dHCP. All of the fetal brain images showed appropriate appearances for their gestational age with no acquired lesions or congenital malformations. The data underwent dynamic geometric correction for distortions, slice-to-volume motion correction[20,21] and temporal denoising[22], followed by their registration to a common space to enable group-level analyses[6].

The framework

In order to demonstrate the utility of our approach, we note that developmental changes in a spatial layout of functional networks can be modelled retrospectively within the standard group-ICA approach using several post-processing steps[14], as shown in Figure 1A. The results of this modelling can provide a benchmark for a comparison with matnets. In brief, the modelling involves the estimation of group-level ("canonical") spatial maps, followed by the two steps of dual regression (DR)[14], i.e., a sequence of spatial and temporal regressions performed against individual data, in order to obtain subject-specific variants of the group maps, followed by a mass-univariate (i.e., voxelwise) modelling of the latter using age as a covariate. The key step is the dual regression step, that "permits the identification of between-subject differences in resting functional connectivity based on between-subject similarities"[14], where a subject-specific map represents the individualised manifestation of a group map. In contrast, our matnets approach, shown in Figure 1B, attempts to derives maps of maturational modes of variation in a direct manner, in essence by reversing the order of operations while omitting the intermediate steps of dual regression. It runs as follows. At the first step, a dense N voxels by N voxels connectome is computed for each subject separately. Each element of the dense connectome is then fitted across subjects with age as covariate, and converted into a t-weighted dense connectome, i.e., a matrix in which elements contain the estimates of the age effect. An ICA factorisation of the t-

weighted connectome is then performed to factorise matnets that comprise voxels with similar maturational profiles across the study period.

(A)

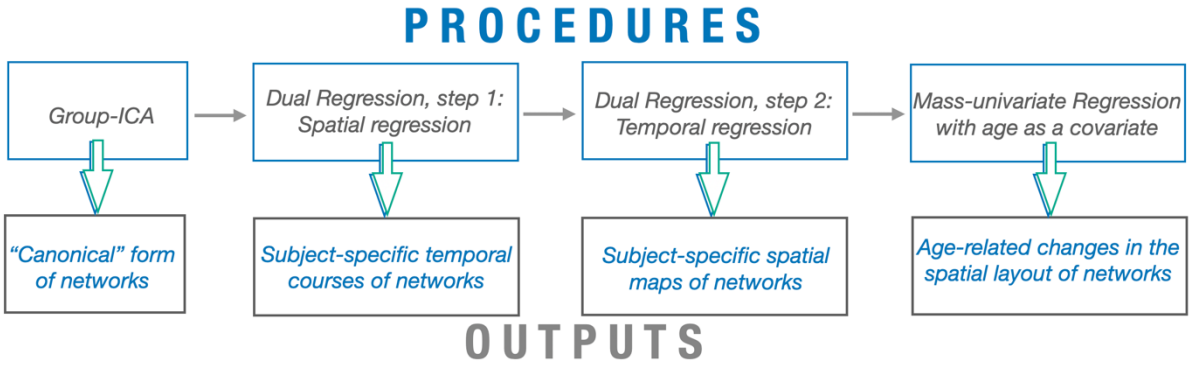

(B)

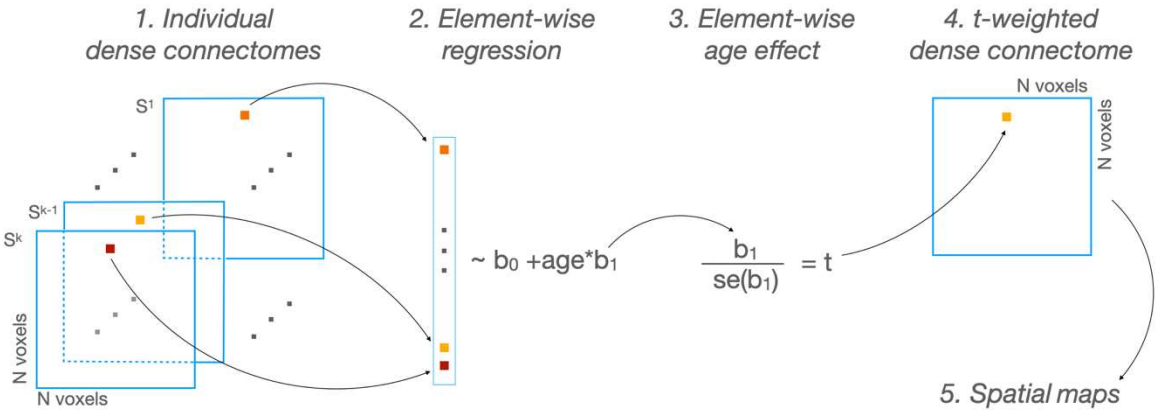

Figure 1. Two approaches to maturational analysis of the functional networks. (A) Group-ICA + dual regression pipeline and its outputs. The pipeline allows modelling maturational changes in the spatial layout of the networks using mass-univariate analysis of the subject-specific variants of the group maps. The latter are derived using dual regression. (B) Pipeline for derivation of maturational networks. It directly leverages age-related changes to derive networks instead of estimating subject-specific variants of the group-level maps. se – standard error

Univariate spatial properties of group-average correlations and age-related differences in correlations

The efficiency of either method for network analysis, for instance in terms of their ability to discover meaningful spatial relationships, is contingent on the relevant signal properties of the data, which remain poorly understood for the in-utero fMRI. A brief description of these properties would assist subsequent interpretations and inform analytical choices. Consequently, we provide a short summary of the univariate spatial properties of the two metrics that are expected to shape the results of the group-ICA and matnets analyses: respectively, group-average correlations and the effect of age (t-value) on the strength of correlations.

The generic spatial structure of the two metrics can be easily appreciated by considering connectivity maps from seed regions to the whole brain ("seed-to-brain" maps). The maps of the group-average correlation for six cortical seeds (3 per hemisphere) are shown in Figure 2A. The conspicuous feature of these maps is a presence of a strong distance dependent gradient, indicating signal smearing over the immediate neighbourhood of the seed. This effect transgresses anatomical boundaries, as demonstrated in a context where the anatomical and purely spatial distances can be disentangled (Supplementary Figure 2) and shows a spatially indiscriminate character as it could equally be replicated for seeds located in the white matter (Supplementary Figure 3).

In comparison, the configuration of the spatial maps for the age-related effect on correlation for the same set of seeds reveals two components of relevance: a negative local component and a positive mid- and long-distance component (Figure 2B). The negative local component is revealed by a distribution of high negative values in the proximity of the seed. This local component, which implies that the strength of distance-dependent gradients in connectivity structure is negatively associated with age at a short distance, occurs in a spatially indiscriminate manner (Supplementary Figure 4), though less obviously in white matter, possibly due to a greater signal blurring within this tissue. Otherwise, the positive mid- and long-distance component is characterised by an age-related increase in correlation strength between seed and other grey matter regions.

Furthermore, the spatial distance also determines a similarity (i.e., spatial correlation) between pairs of maps (Figure 2C) for group-average correlation, which suggests that spatial distance may become a dominant factor for the fusion of the voxels into networks in the analyses based on the correlational structure of the data, such as group-ICA. Conversely, the same figure (Figure 2C) also shows that the similarity between age-effect maps was unaffected by the spatial distance between seeds used to produce these maps. This suggests that leveraging positive age-related associations for the network construction can potentially reveal a rich set of spatially distributed patterns with improved specificity. In this view, matnets were derived using a factorisation of the positively thresholded t-weighted connectome.

(A)

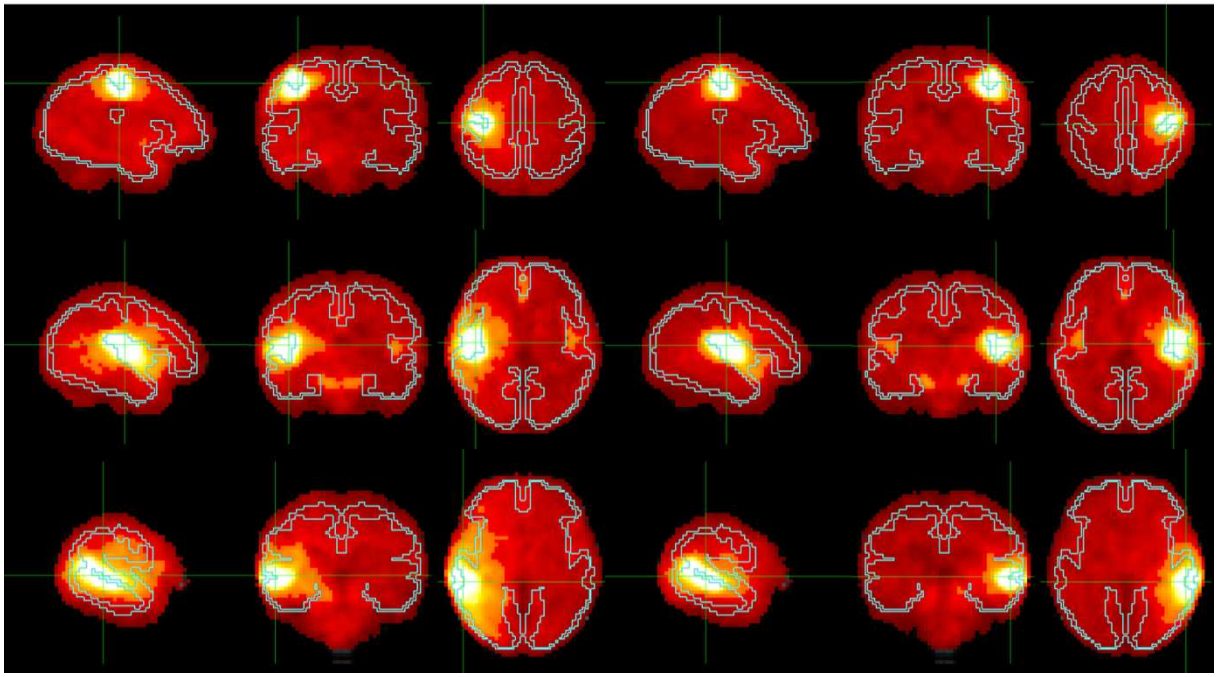

(B)

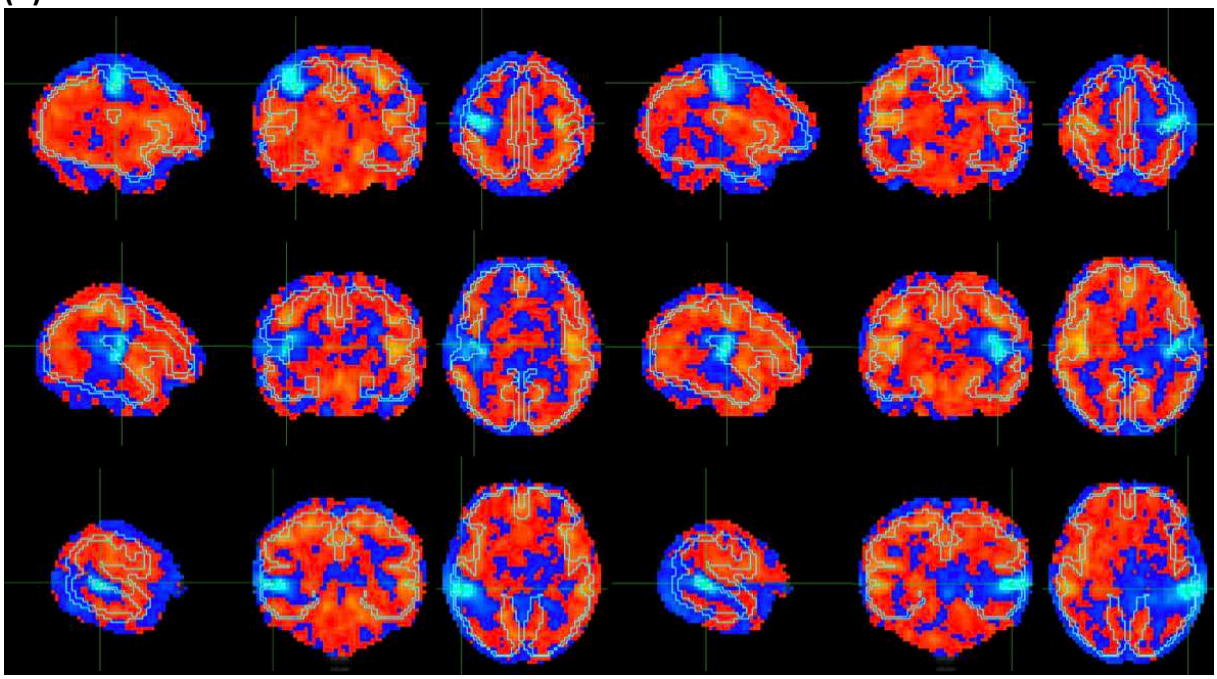

(C)

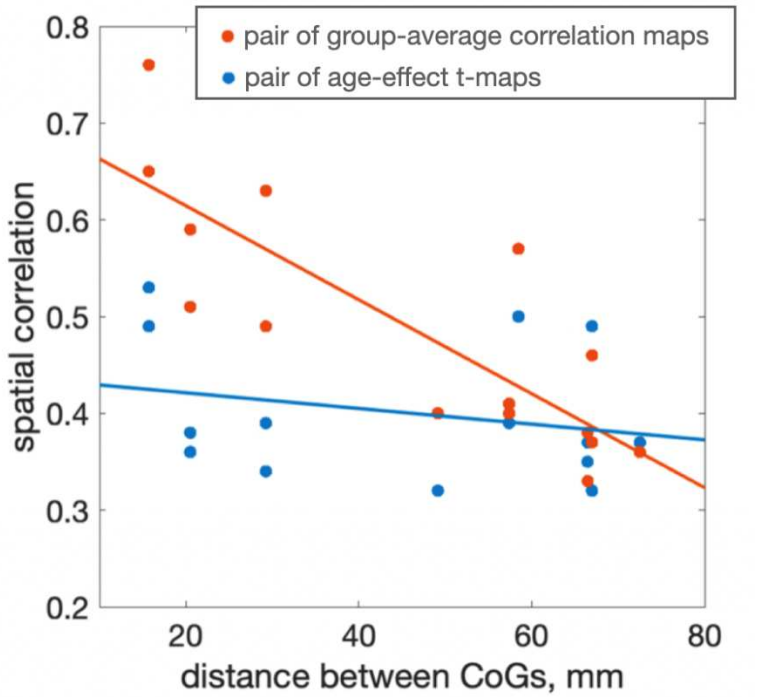

Figure 2. Spatial properties of group-average correlations and age-related differences in correlations. All spatial maps are shown in radiological orientation, i.e., left is right. (A) seed-to-brain maps of group-average correlations. Location of a seed coincides with a center of the crosshair. Examples of 6 seeds are shown, 3 per each hemisphere (B) Same as (A) for the age-effect maps. (C). Spatial similarity between each pair of seed-to-brain maps. CoG – centre of gravity. Statistical testing of 2 main effects (type of map and distance) and their interaction shows a significant main effect of type of map (i.e., higher spatial correlation for the group-average correlation maps, $t(26) = 4.30$, $p < .001$), and a significant interaction between distance and type of map (i.e., higher dependency on the distance the group-average correlation maps, $t(26) = 3.21$, $p < .005$), but not the main effect of distance ($p = 0.37$, i.e., indicating a relative tolerance of the age effect statistics to the factor of spatial distance).

Group ICA maps and estimated age-related differences in their layout

The results of group-ICA factorisation are shown in Figure 3A. The appearance of the spatial maps suggest that they inherit certain signal properties that had previously been revealed in the univariate analysis. Thus, their "blurry" appearance is reminiscent of the increased local signal correlations observed in univariate maps of seed-to-brain group-average correlations. In addition, the location of the peaks in many group-ICA maps tended to be biased away from the cortex towards the white matter and a local low-to-high ramp of the component values could often be traced along the boundary between grey and white matter tissues (Supplementary Figure 5). Despite the above characteristics, most components have anatomically plausible layouts, encompassing a diverse range of functionally relevant areas. The components where peaks were most firmly located within cortical ribbon, were found in sensorimotor and pre-motor areas (e.g., components #16,17, 23, 24).

Meanwhile, the analysis of age-related changes in the spatial layout of the networks using the dual regression approach appear to be affected by a specific bias, as shown using the examples of the spatial maps of the first 3 components and the corresponding maps of the age effect in Figure 3B, demonstrating a negative effect of age (i.e., a decrease of connectivity with age) in the most representative component voxels. This somewhat counter-intuitive pattern was observed for all group-ICA components. Furthermore, as

Figure 3C shows, there was a high negative spatial correlation between component group-lCA component spatial maps and corresponding t-maps of the age effect. As we will discuss later, this pattern appears to be a direct consequence of the signal properties earlier highlighted in the context of the univariate analyses, showing that there is a negative association between age and strength of correlations for voxels surrounding a seed.

(A)

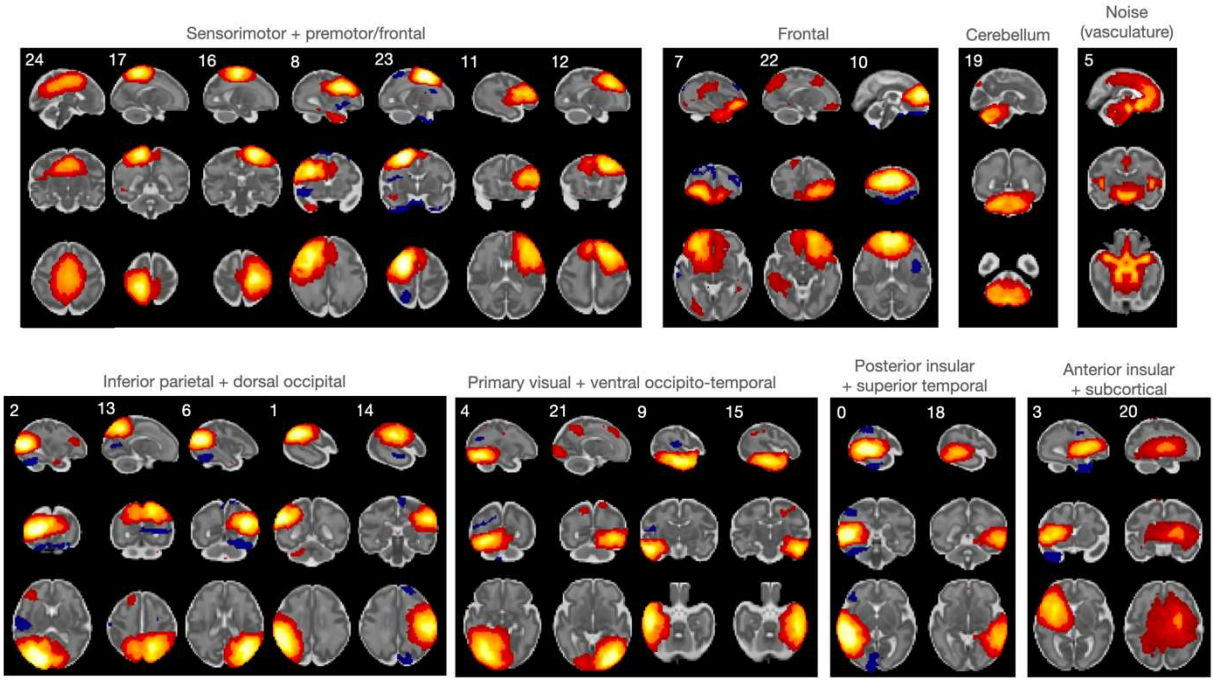

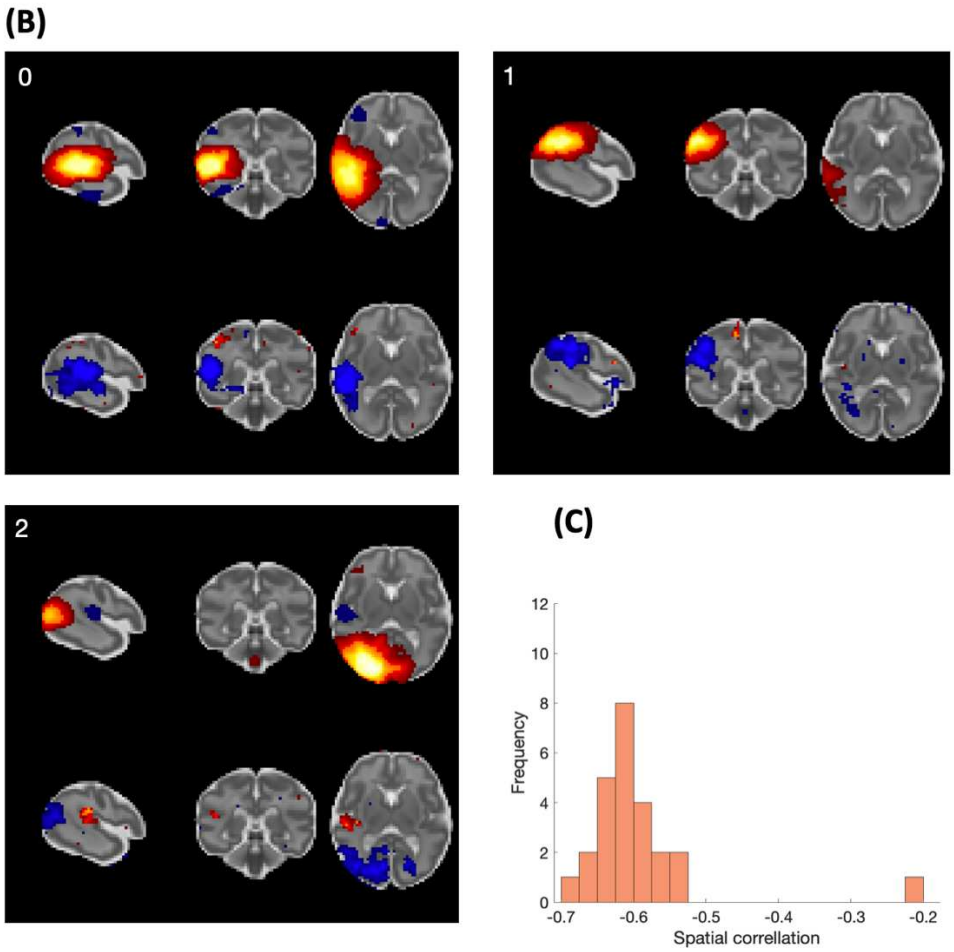

Figure 3. Results of group-ICA analysis. All spatial maps are shown in radiological orientation. (A) Group-level spatial maps, thresholded at abs(z) >3. (B). Spatial maps of the first 3 components (upper row) and the corresponding maps of the age effect (lower row). A negative effect of age can be observed in the most representative component voxels. (C) Distribution of spatial correlations between component spatial maps and corresponding t-maps. The outlier is the component with likely vascular origin (#5 in (A))

Maturational networks (matnets)

The above analysis demonstrates an inability to reconstruct coherent maturational relationships in the fetal fMRI data using tools that are widely used in standard network analysis in pediatric and adult populations. In contrast, results from the maturational network factorisation, presented in Figure 4A, reveal spatial configurations of a high anatomical validity, including locality within the grey matter (Supplementary Figure 6). In order to ascertain the robustness of the method, we repeated the analysis in split-half samples. We found a good replicability of the network properties (Supplementary Figures 7 and 8), including non-trivial connectivity patterns, such as between the occipito-temporal and dorsal somatosensory/superior parietal cortices and between the right anterior lateral temporal and right dorsolateral pre-motor/pre-frontal cortices. Compared to the group-ICA, the matnets tended to show a greater spatial complexity, encompassing non-adjacent areas. For instance, the main node of matnet #11 spatially overlapped with that of group-ICA #24

but in addition encompassed areas in lateral central and pre-motor cortices. Another example is the bilateral matnet component #7 in which the left-hemisphere sub-division overlapped with a spatially compact group-ICA component #16. Furthermore, the matnet maps tended to demonstrate more anatomically specific local variations of intensity compared to the group-ICA maps (Figure 4B) which are reminiscent of the spatial specificity in the age-effect seed-to-brain maps from the univariate analyses. For instance, the matnet map #7 in Figure 4B has multiple poles, distributed across the somatosensory, motor and premotor cortices, which suggests an early integration of local circuits supporting different functions. In contrast, group-ICA components were typically characterised by the tendency to have one centre-of-gravity.

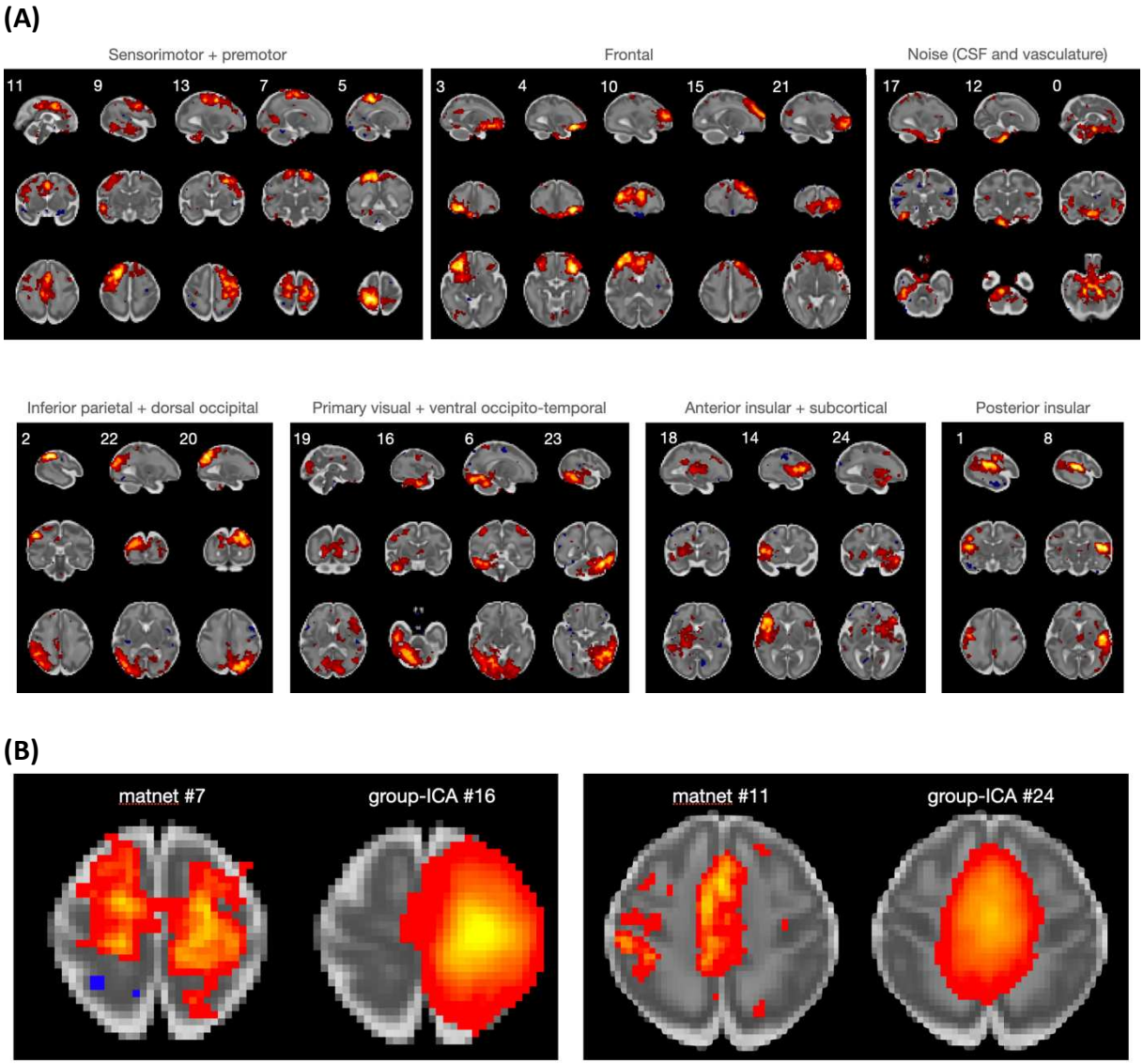

Figure 4. Results of maturational network analysis. All spatial maps are shown in radiological orientation. (A) Spatial maps. (B) Examples of components from maturational and group-ICA analyses, showing that the former tends to show more anatomically specific variation in intensity than the latter.

Whole-brain maturational connectome

In order to complete the description of the maturational relationships, we present a whole-brain view of the in utero functional architecture, i.e., the fetal brain's functional connectome. Within the standard group-ICA+DR approach, the functional connectome is described using "netmats"[26], a matrix of correlations between component timecourses estimated in step 1 of DR. Our goal here is to present a maturational analogue to this approach, which we refer to as a "maturational connectome". We estimate it using the outputs provided by the framework of the maturation network analysis, as shown in Figure 5A. In brief, it involves the regression of the maturational networks against columns of the thresholded t-weighted connectome in order to obtain a N components by N voxels matrix of estimated regression coefficients (an analogue of component timecourses of DR1), followed by calculation of N components by N components matrix, in which elements represent correlations between each pair of rows in the regression coefficient matrix. The latter matrix constitutes the maturational connectome.

A three-dimensional embedding of the maturational connectome (Figure 5B), allows one to appreciate its generic structure. Here a point in space indicates a relative location of a network with respect to other networks, with a shorter distance between networks being indicative of stronger maturational ties (i.e., maturing together). 5 groups of networks can be identified using hierarchical clustering, based on the networks' location in the embedded space (Figure 5C). The first ("red") group consisted of networks that combined the posterior and anterior peri-insular areas with occipital, auditory and ventral sensorimotor areas. The second ("green") group consisted of two smaller sub-groups: one comprising dorsolateral pre-motor, dorsolateral prefrontal and medial pre- and supplementary motor areas; the other combining frontal anterior cingulate with inferior parietal and superior lateral occipital cortices, extending into medial posterior areas (precuneus). Adjacent to this group, there was a two-network ("blue") group, comprising dorsal sensorimotor areas. The fourth ("violet") group comprised ventral frontal and orbitofrontal areas. Finally, the last ("purple") group combined ventral occipito-temporal areas with dorsal parietal and sensorimotor areas.

(A)

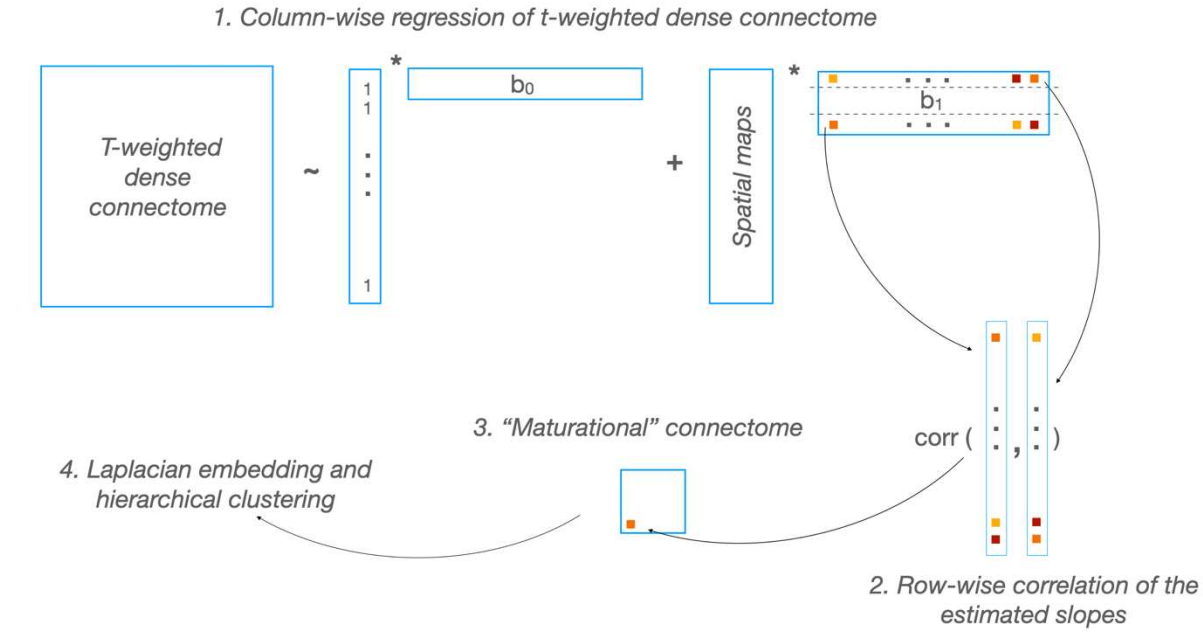

(B)

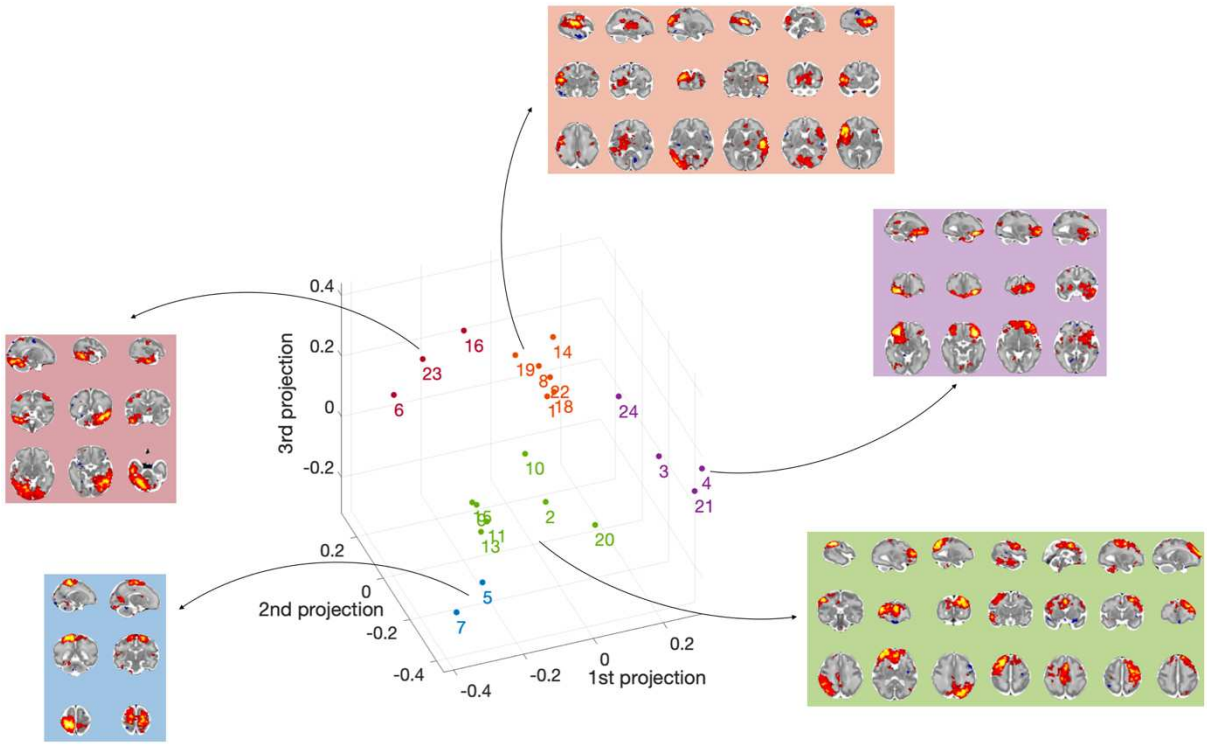

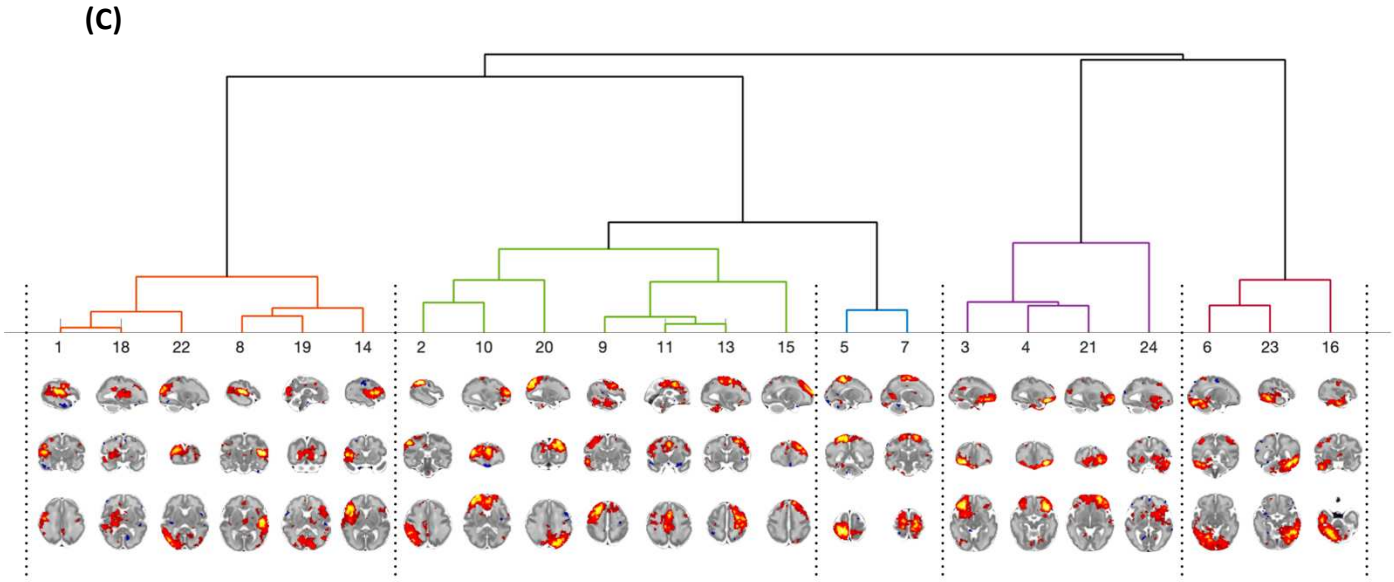

Figure 5. Maturational connectome. (A) Pipeline for derivation and analysis of maturational connectome (B) Maturational connectome embedding and their split into groups, based on hierarchical clustering (C) Hierarchical clustering tree.

DISCUSSION

In this paper we present a framework for characterising in-utero functional brain architecture that models networks as an emerging property of the brain. Within this framework, which we call maturational network analysis, the fusion of voxels into a network is determined by the similarity of their maturational profiles with respect to the rest of the brain. In effect, this represents a computational implementation of Flechsig's principle[17] that states that concordant maturation characterises functionally related areas.

In an implicit form, Flechsig's principle has been previously utilised in the studies of structural covariance[27] in developmental cohorts[28,29], including fetal ones[30]. Here we apply the principle explicitly to the study of brain's functional organisation.

We have found several key methodological benefits of maturational network analysis in the context of the fetal resting-state fMRI data. First, we have demonstrated the robustness of the method by showing a persistence of the network properties in split-half subsamples. Next, we have showed that maturational networks represent a coherent way of characterising maturational patterns in the context of fetal fMRI, compared to inference using the standard approach, in which results appear to be affected by a specific bias (we will discuss this below). Matnets have revealed spatially distributed patterns of connections with a remarkable anatomical specificity for the in-utero data likely owing to their reliance on the benign signal properties that reveal an age-dependent increase of mid- and long-distance connectivity in a spatially selective manner. Finally, the framework renders biologically interpretable results, reflecting a range of motifs characteristic of the neonatal brain connectivity, which can be viewed as the eventual target for maturational processes in utero. Thus, several networks revealed a non-negligible bilateral component, that agrees with the studies of pre-term and term born babies [4-6] as well as in-utero seed-based

connectivity fMRI studies[8] suggesting that interhemispheric coupling becomes established during this period. The maturational networks also characterised a range of non-trivial functional relationships that are similarly observed in neonatal data[6], such as functional associations between the inferior parietal regions and precuneus; between the anterior cingulate cortex and lateral orbito-frontal cortex, between the medial and lateral (pre)-motor cortices; between the central sulcus and posterior insular cortex; or between the dorsal and ventral stream regions. This demonstrates that these emerging functional relationships across spatially distinct regions are an intrinsic property of the brain and provides crucial validation of the findings of neonatal studies where the complementary role of environmental influences had been unclear.

An additional level of insight into the developmental sequelae of the fetal functional brain is provided by a low-dimensional embedding of the whole-brain maturational connectome, allowing an appreciation of mutual relationships between networks. A conspicuous generic feature of this connectome is the tendency for homologous contralateral networks to cluster together. Overall, the clustering analysis identifies two larger groups that occupy the central location in the maturational connectome and three smaller, more peripheral, groups. Based on the areas that dominate their anatomical layout, the three smaller clusters of networks can be labelled as orbitofrontal, ventral visual and sensorimotor groups. Of the larger groups, one was dominated by the cortical nodes of perception and bodily sensation (occipital, auditory and somatosensory limbic areas) but also included nodes in the motor and motor limbic[31] (anterior cingulate and anterior insular) cortices. The other larger group was dominated by the functional nodes responsible for an environmental interaction through action (dorsolateral and medial pre-motor cortex and pre-frontal areas), but also included a sub-group of networks which spatially overlap with nodes of the future default mode networks[23,32], such as precuneus, anterior cingulate and angular gyrus. Notably, the location of the latter within the embedding space was midway between the notional perception group and the remaining networks of the notional action group, hinting both towards hub connectivity patterns and their apparent role in modulating internal and external inputs whilst mind-wandering or performing cognitively demanding tasks later in life[33].

Compared to maturational networks, group-ICA components identified with a standard group-ICA approach had diminished spatial complexity and anatomical specificity and were biased towards the white matter. Notably, the results of dual regression modeling showed that local connectivity within group-ICA networks diminishes with age. Such characteristics fit well those of the functional nodes described in the fetal animal studies, which center on the cortical subplate and act as local amplifiers of the thalamic activity with spread that does not conform to anatomical boundaries[3,34]. This may suggest that group-ICA and maturational networks truthfully reflect two different states of the fetal functional brain: a truly “fetal” subplate-centered[35] and locally active state depicted by the group-ICA, that gives way to the adult-like cortex-centered and spatially distributed state of maturational networks.

Against this intriguing interpretation, though not necessary incompatible with it, are the results of the univariate analysis of the connectivity metrics. The latter demonstrates that the correlational structure of the data, that underlies the derivation of the group-ICA components, is dominated by a spatially smooth and non-linear distance-dependent

gradient, which at a short distance is scaled negatively with age. The factors that make biologically-motivated interpretation of this gradient unlikely is the spatially indiscriminate character of these phenomena combined with a violation of anatomical boundaries, including the large connectivity distance between the two brain hemispheres which in reality are separated by a CSF filled inter-hemispheric fissure.

An initial hypothesis to explain the origins of distance-dependent gradients and its interaction with age can be based on the potential contribution of two factors: motion and effective resolution. The role of motion on connectivity estimates has been demonstrated in adult imaging, where it has been shown to decrease long-range connectivity and overestimate local connectivity[36,37]. Although we used a comprehensive image processing pipeline to account for head motion during data acquisition, fetal imaging data is still especially susceptible to this effect as it has virtually no motion-free periods. Even if the fetus stays still, maternal breathing cycles and endogenous motion in the non-rigid tissues surrounding the fetal head continue to cause a constant change of position. Under these circumstances, effective resolution naturally leads to age-related differences in the effect, which likely explains the dual regression result showing a decrease in connectivity with age within the most representative component voxels. The brain undergoes a 3-fold growth in size over the studied period, which implies that real-world separation between pairs of voxels in the standard space is smaller for younger subjects than for older ones and thus a greater effect of distance as measured in the common space. In light of the differences in signal properties between the grey and white matter and their modulation by age, the possible contribution of other factors such as modulation of the BOLD signal itself and/or the role of age-related changes in tissue content should also not be disregarded.

A question can also be asked about the biological underpinnings of the age-related increase in correlation implicated in the derivation of maturational networks. Maturation entails competing physiological processes which may potentially leave a footprint on the properties of the fMRI signal[38,39]. For instance, one cannot exclude the possibility that changes in the long-distance connectivity are in part due to the coordinated development of the brain's vasculature[40]. De-confounding the latter from the estimates of neural connectivity is a contentious issue even in the context of adult resting-state imaging[41,42]. In the fetal brain the problem may be further exacerbated as the development of brain neural systems goes hand in hand with the development of other organ functions and therefore the development of vascular and activity-dependent components are likely collinear to the degree that the two are indistinguishable at a level visible to fMRI.

Below we outline several limitations of the study. First, the current study has the well-known limitations of cross-sectional analyses whereby between-subject variability can be confounded with aging effects. Nevertheless, cross-sectional data are expected to dominate the fetal research for a foreseeable future, as the problem of scanning mothers during pregnancy multiple times encounters certain ethical and practical challenges. In the meantime, one can strive for better estimates of cross-sectional trajectories, using improved modelling and larger data samples. Our results are based on the largest fetal fMRI data set both in terms of the number of subjects and the number of volumes per subject. However, further improvements in modelling can be achieved when data for the full fetal dHCP cohort will be made openly available to the neuroscientific community in the coming year. This

would increase the current data sample by a factor nearing to 2. In addition, it is expected to contain more than 20 participants scanned twice, a potential starting point for longitudinal studies.

The second limitation concerns generalisation of our conclusions to other data samples, especially in the context of fetal fMRI as a novel field, where norms of data acquisition are yet to be established. Unfortunately, fetal fMRI has not as yet stepped in into the age of normative open-access big data[43] which has enabled recent progress in the study of ex-utero connectivity, (e.g.,[44]). However, the qualitative comparison of our results with the results drawn from other studies gives us a certain confidence that our results are not specific to our sample. For instance, there was a remarkable similarity between our group-ICA results and the group-ICA results reported in a recent paper[11], despite considerable differences in the acquisition sequence (multi- vs single-band), spatial image corrections (dynamic distortion and slice-to-volume corrections vs volumetric alignment only) and de-noising pipelines (predominantly motion parameter-based vs. ICA-based). Furthermore, the qualitative characteristics of group-ICA components as well as the dominance of distance-dependent gradient over the correlational structure also appear to be reproducible across the studies[11].

In conclusion, we have described a novel framework that can characterise the spatial distribution of maturing functional networks which has been applied to delineate the emergence of resting state networks in the fetal human brain. A discerning feature of this maturational network framework is a prospective incorporation of the variable-of-interest (here, age) into network estimation. This can potentially make the method adaptable to other problems, such as early human development through infancy, network maturations in neurodevelopmental disorders, such as autism, ageing and exploring connectivity underpinnings of behavior.

METHODS

Data

Resting-state fMRI data were acquired in 151 fetuses (62 females, 77 males, 5 unknown), median age = 29.5w, range = [25 38], with Philips Achieva 3T system (Best, NL) and a 32-channel cardiac coil. Single-shot EPI (TR/TE = 2200/60) sequence consisted of 350 volumes of 48 slices each, slice grid 144 x 144, isotropic resolution = 2.2 mm, multi-band (MB) factor = 3 and SENSE factor = 1.4[25]. All of the fetal brain images were reported by a neuroradiologist as showing appropriate appearances for their gestational age with no acquired lesions or congenital malformations of clinical significance. Data from 7 fetuses did not pass quality control assessment due to excessive motion and failure in image reconstruction.

The data of the remaining 144 fetuses were preprocessed using a dedicated pipeline[21,22]. In brief, the data underwent MB-SENSE image reconstruction, dynamic shot-by-shot B0 field correction by phase unwrapping and slice-to-volume (S2V) motion correction. A temporal denoising model, optimised for ability to both recover signal and minimise risk of its inadvertent removal, was then applied to the data. The model combined volume censoring

regressors, aiming to reject volumes (at a heuristically selected threshold) (Supplementary Figure 9), highpass (1/150 Hz) filtering regressors of direct cosine transform matrix in order to remove slow frequency drift in the data, 6 white matter and cerebrospinal fluid component timecourses (obtained using subject-level ICA within a combined white matter + CSF mask, e.g.,[45]), and 3 novel variants of voxelwise denoising maps in order to account for the local artefacts in the data: 1) folding maps (N=2) which aggregate time courses of voxels linked in multiband acquisition to voxels in the original data, aiming at filtering out leakage artefacts; 2) density maps, representing temporal evolution of an operator that compensates for the volume alterations a result of distortion in phase encoding direction, and aiming to filter out residual effects of distortion correction on the voxel timecourses; and 3) motion-parameter-based (MP-based) regressors, expanded to include first and second order volume-to-volume and slice-to-slice differentials as well as their square terms, aiming to remove motion-related artefacts[46,47].

Registration to the group space

A schematic depiction of the registration to a common template space is shown in Supplementary Figure 10. The mapping between a functional native space and the common template space is constructed as the concatenation of several intermediate transformations, which ascertain a gradual alignment between spaces to minimise the risks of gross misalignment as a result of the substantial differences in the brain topology across the range of gestation ages[6]: 1) rigid alignment between mean functional and anatomical scans calculated using FLIRT[48]; 2) a non-linear transformation between an anatomical T2 scan and an age-matched template[49] (available at https://brain-development.org/brain-atlases/fetal-brain-atlases/) calculated using ANTs[50] ; 3) a sequence of non-linear transformations between templates of adjacent ages (e.g., 24 and 25, 25 and 26, etc.), also calculated using ANTs. These transformations were concatenated to create a one-step mapping between functional and group template space, avoiding multiple interpolations. The template corresponding to GA=37 was selected as a common space for group analysis based on the considerations that it has a greatest effective resolution and topological complexity. An additional group space was created by symmetrizing the GA=37 template with respect to the brain midline, with appropriate adjustment of the mapping from the functional native spaces, that included an additional non-linear transform from non-symmetrical-to-symmetrical template spaces. After registering the functional MRI data to the template space, they were smoothed using 3mm Gaussian kernel.

Data analysis

Univariate analyses. The seeds for the seed-to-brain analysis were determined empirically using the results of modelling age-related changes in interhemispheric connectivity between pairs of homologous voxels (Supplementary Figure 11), performed in the symmetrical template space[25]. The subject-specific maps of homologous voxel connectivity were obtained by calculating the correlation between timecourses of homologous voxels in the two hemispheres. The age-effect map was obtained via a voxel-wise regression with age as a covariate. The seeds for grey matter were created by thresholding the age-effect map from the above analysis at $z > 3$, which rendered 3 sizable clusters of voxels (14, 32 , and 45 voxels). Given the absence of positive age-related increase in connectivity between

homologous voxels for white matter areas, the white matter seeds were created by thresholding the age-effect map of interhemispheric connectivity negatively at $z < -3$, and then manually adjusting clusters to fit the size of the grey matter clusters. Because the seeds were defined in the symmetrical template space, the seed-to-brain connectivity analysis was also performed in this space. The seed-to-brain group-average correlation map was calculated by first calculating individual maps of correlations between time course of a seed and time courses of all voxels in the brain and then averaging these maps across subjects. The age-effect map was obtained by fitting individual maps voxelwise using age as a covariate.

Group-ICA. The derivation of group-average modes-of-variation and their subject-specific variants was performed using the protocol of FSL MELODIC for group-ICA analyses[15], including FSL MELODIC's Incremental Group Principal component analysis (MIGP step[12]), and the standard procedure of dual regression, implemented in FSL[51]. The number of derived components was set to 25.

Maturational modes of variation. The pipeline for derivation of maturational modes of variation is shown in Figure 1B. First, a symmetrical matrix of correlations between each pair of voxels in the brain mask was calculated, aka "dense connectome", for each subject separately. Each element of the dense connectome was fitted across subjects with age as covariate, rendering a voxel-by-voxel matrix of age-effect beta coefficients. The matrix was then converted into t-values, rendering t-weighted dense connectome, subsequently thresholded at 0 in order to leverage the age-dependent increases in correlations in network estimation. The rationale for positive thresholding is described in Results section. In order to perform connectome factorisation, an intermediate step of dimensionality reduction, analogous to MIGP, was applied. For this, the t-weighted dense connectome (size: N voxels by N voxels) was split column-wise into 200 blocks (size: N voxels by N voxels/200. At the initial step, a matrix consisting of the first two blocks was formed and subsequently reduced to 500 components using singular value decomposition. An iterative procedure was then run that consisted of concatenating the current matrix of 500 components with a following block and subsequent reduction to 500 components by SVD, until all blocks were exhausted. The output of this procedure was used to obtain the final factorisation of 25 components using FSL MELODIC.

Maturational connectome analysis. The pipeline for derivation of the maturational connectome is shown in Figure 5A. It consists of the regression of the maturational networks against the t-weighted dense connectome in order to obtain #networks by #voxels matrix of regression coefficients. Correlations between each pair of rows of the matrix were then estimated, collected into a matrix which constitutes the maturational connectome. In order to unveil a structure of the whole-brain maturational relationships, the maturational connectome matrix was embedded into 3-dimensional space using an eigendecomposition of a graph normalised Laplacian. A point in the embedding space indicates a relative location of a network with respect to other networks (i.e., a shorter distance means closer maturational ties). In order to facilitate the discussion of results, a partition of networks into groups of networks was performed using the Ward method of hierarchical clustering[52], based on the network coordinates in the embedding 3D space.

Funding

The Developing Human Connectome Project was funded by the European Research Council under the European Union Seventh Framework Programme (FP/20072013)/ERC Grant Agreement no. 319456. The authors also acknowledge support in part from the Wellcome Engineering and Physical Sciences Research Council (EPSRC) Centre for Medical Engineering at Kings College London [WT 203148/Z/16/Z], the Medical Research Council (MRC) Centre for Neurodevelopmental Disorders [MR/N026063/1], and the Department of Health through an NIHR Comprehensive Biomedical Research Centre Award (to Guy's and St. Thomas' National Health Service (NHS) Foundation Trust in partnership with King's College London and King's College Hospital NHS Foundation Trust). VK and TA were additionally supported by a MRC Clinician Scientist Fellowship [MR/P008712/1] and MRC translation support award [MR/V036874/1]. JOM is supported by a Sir Henry Dale Fellowship jointly funded by the Wellcome Trust and the Royal Society [Grant Number 206675/Z/17/Z]. LCG is supported by the Comunidad de Madrid-Spain Support for R&D Projects [BGP18/00178]. AEF acknowledges additional funding from the UKRI CDT in Artificial Intelligence for Healthcare in his role as a Senior Teaching Fellow [grant number EP/S023283/1]

REFERENCES:

1 Kant, I. *Critique of Pure Reason*. (Penguin Classics, 2007).
2 Nietzsche, F. *The Birth of Tragedy*. (Penguin Classics, 1993).
3 Khazipov, R. & Luhmann, H. J. Early patterns of electrical activity in the developing cerebral cortex of humans and rodents. *Trends Neurosci* **29**, 414-418, doi:10.1016/j.tins.2006.05.007 (2006).
4 Doria, V. *et al.* Emergence of resting state networks in the preterm human brain. *Proc Natl Acad Sci U S A* **107**, 20015-20020, doi:10.1073/pnas.1007921107 (2010).
5 Eyre, M. *et al.* The Developing Human Connectome Project: typical and disrupted perinatal functional connectivity. *Brain* **144**, 2199-2213, doi:10.1093/brain/awab118 (2021).
6 Fitzgibbon, S. P. *et al.* The developing Human Connectome Project (dHCP) automated resting-state functional processing framework for newborn infants. *Neuroimage* **223**, 117303, doi:10.1016/j.neuroimage.2020.117303 (2020).
7 Gould, S. J. *Ontogeny and Phylogeny*. (Belknap Press of Harvard University Press, 1985).
8 Thomason, M. E. *et al.* Cross-hemispheric functional connectivity in the human fetal brain. *Sci Transl Med* **5**, 173ra124, doi:10.1126/scitranslmed.3004978 (2013).
9 Thomason, M. E. *et al.* Age-related increases in long-range connectivity in fetal functional neural connectivity networks in utero. *Dev Cogn Neurosci* **11**, 96-104, doi:10.1016/j.dcn.2014.09.001 (2015).
10 Ferrazzi, G. *et al.* Resting State fMRI in the moving fetus: A robust framework for motion, bias field and spin history correction. *Neuroimage* **101**, 555-568 (2014).
11 Ji, L., Hendrix, C. L. & Thomason, M. E. Empirical evaluation of human fetal fMRI preprocessing steps. *Network Neuroscience*, 1-37, doi:10.1162/netn_a_00254 (2022).

12 Smith, S. M., Hyvarinen, A., Varoquaux, G., Miller, K. L. & Beckmann, C. F. Group-PCA for very large fMRI datasets. *Neuroimage* **101**, 738-749, doi:10.1016/j.neuroimage.2014.07.051 (2014).

13 Calhoun, V. D., Adali, T., Pearlson, G. D. & Pekar, J. J. A method for making group inferences from functional MRI data using independent component analysis. *Hum Brain Mapp* **14**, 140-151, doi:10.1002/hbm.1048 (2001).

14 Beckmann, C. F., Mackay, C. E. & Smith, S. M. Group comparison of resting-state FMRI data using multi-subject ICA and dual regression. *NeuroImage* **47**, S148, doi:10.1016/S1053-8119(09)71511-3 (2009).

15 Beckmann, C. F. & Smith, S. M. Probabilistic independent component analysis for functional magnetic resonance imaging. *IEEE Trans Med Imaging* **23**, 137-152, doi:10.1109/TMI.2003.822821 (2004).

16 Bijsterbosch, J. D. *et al.* The relationship between spatial configuration and functional connectivity of brain regions. *Elife* **7**, doi:10.7554/eLife.32992 (2018).

17 Flechsig, P. Developmental (myelogenetic) localisation of the cerebral cortex in the human subject. *Lancet* **158**, 1027-1030, doi:10.1016/S0140-6736(01)01429-5 (1901).

18 Edwards, A. D. *et al.* The Developing Human Connectome Project Neonatal Data Release. *Frontiers in Neuroscience* **16**, doi:10.3389/fnins.2022.886772 (2022).

19 http://www.developingconnectome.org.

20 Cordero Grande, L., Price, A. N., Christiaens, D., Hutter, J. & Hajnal, J. V. Spin And Field Echo (SAFE) dynamic field correction in 3T fetal EPI. In *Proceedings of the 26th annual meeting of the ISMRM.* 208. (2018)

21 Cordero-Grande, L., Hughes, E. J., Hutter, J., Price, A. N. & Hajnal, J. V. Three-dimensional motion corrected sensitivity encoding reconstruction for multi-shot multi-slice MRI: Application to neonatal brain imaging. *Magn Reson Med* **79**, 1365-1376, doi:10.1002/mrm.26796 (2018).

22 Karolis, V. *et al. Approaches to the in-utero fMRI denoising in the developing Human Connectome Project (dHCP).* In *Organisation for Human Brain Mapping.* 2112. (2021).

23 Smith, S. M. *et al.* Correspondence of the brain's functional architecture during activation and rest. *Proc Natl Acad Sci U S A* **106**, 13040-13045, doi:10.1073/pnas.0905267106 (2009).

24 Damoiseaux, J. S. *et al.* Consistent resting-state networks across healthy subjects. *Proc Natl Acad Sci U S A* **103**, 13848-13853, doi:10.1073/pnas.0601417103 (2006).

25 Price, A. N. *et al.* The developing Human Connectome Project (dHCP): fetal acquisition protocol. In *Proceedings of the annual meeting of the International Society of Magnetic Resonance in Medicine (ISMRM).* 244. (2019)

26 Smith, S. M. *et al.* A positive-negative mode of population covariation links brain connectivity, demographics and behavior. *Nat Neurosci* **18**, 1565-1567, doi: 10.1038/nn.4125 (2015).

27 Mechelli, A., Friston, K. J., Frackowiak, R. S. & Price, C. J. Structural covariance in the human cortex. *J Neurosci* **25**, 8303-8310, doi: 10.1523/JNEUROSCI.0357-05.2005 (2005).

28 Fenchel, D. *et al.* Development of Microstructural and Morphological Cortical Profiles in the Neonatal Brain. *Cereb Cortex* **30**, 5767-5779, doi:10.1093/cercor/bhaa150 (2020).

29 Karolis, V. R. *et al.* Volumetric grey matter alterations in adolescents and adults born very preterm suggest accelerated brain maturation. *Neuroimage* **163**, 379-389, doi:10.1016/j.neuroimage.2017.09.039 (2017).

30 Xia, J. *et al.* Fetal cortical surface atlas parcellation based on growth patterns. *Hum Brain Mapp* **40**, 3881-3899, doi:10.1002/hbm.24637 (2019).

31 Craig, A. D. How do you feel? Interoception: the sense of the physiological condition of the body. *Nat Rev Neurosci* **3**, 655-666, doi: 10.1038/nrn894 (2002).

32 Raichle, M. E. *et al.* A default mode of brain function. *P Natl Acad Sci USA* **98**, 676-682, doi:10.1073/pnas.98.2.676 (2001).

33 Raichle, M. E. The Brain's Default Mode Network. *Annu Rev Neurosci* **38**, 433-447, doi: /10.1146/annurev-neuro-071013-014030 (2015).

34 Colonnese, M. T. & Phillips, M. A. Thalamocortical function in developing sensory circuits. *Curr Opin Neurobiol* **52**, 72-79, doi: 10.1016/j.conb.2018.04.019 (2018).

35 Kostovic, I. The enigmatic fetal subplate compartment forms an early tangential cortical nexus and provides the framework for construction of cortical connectivity. *Prog Neurobiol* **194**, 101883, doi:10.1016/j.pneurobio.2020.101883 (2020).

36 Power, J. D., Barnes, K. A., Snyder, A. Z., Schlaggar, B. L. & Petersen, S. E. Spurious but systematic correlations in functional connectivity MRI networks arise from subject motion. *Neuroimage* **59**, 2142-2154, doi: 10.1016/j.neuroimage.2011.10.018 (2012).

37 Van Dijk, K. R. A., Sabuncu, M. R. & Buckner, R. L. The influence of head motion on intrinsic functional connectivity MRI. *Neuroimage* **59**, 431-438, 10.1016/j.neuroimage.2011.07.044 (2012).

38 Harris, J. J., Reynell, C. & Attwell, D. The physiology of developmental changes in BOLD functional imaging signals. *Dev Cogn Neuros-Neth* **1**, 199-216, doi: 10.1016/j.dcn.2011.04.001 (2011).

39 Pietsch, M. *et al.* A framework for multi-component analysis of diffusion MRI data over the neonatal period. *Neuroimage* **186**, 321-337, doi:10.1016/j.neuroimage.2018.10.060 (2019).

40 Lacoste, B. & Gu, C. H. Control of cerebrovascular patterning by neural activity during postnatal development. *Mech Develop* **138**, 43-49, doi: 10.1016/j.mod.2015.06.003 (2015).

41 Bright, M. G., Whittaker, J. R., Driver, I. D. & Murphy, K. Vascular physiology drives functional brain networks. *Neuroimage* **217**, 116907, doi:10.1016/j.neuroimage.2020.116907(2020).

42 Murphy, K., Birn, R. M. & Bandettini, P. A. Resting-state fMRI confounds and cleanup. *Neuroimage* **80**, 349-359, doi: 10.1016/j.neuroimage.2013.04.001 (2013).

43 Rajagopalan, V., Deoni, S., Panigrahy, A. & Thomason, M. E. Is fetal MRI ready for neuroimaging prime time? An examination of progress and remaining areas for development. *Dev Cogn Neuros-Neth* **51**, 100999, doi: 10.1016/j.dcn.2021.100999 (2021).

44 Smith, S. M. *et al.* Resting-state fMRI in the Human Connectome Project. *Neuroimage* **80**, 144-168, doi:10.1016/j.neuroimage.2013.05.039 (2013).

45 Behzadi, Y., Restom, K., Liau, J. & Liu, T. T. A component based noise correction method (CompCor) for BOLD and perfusion based fMRI. *Neuroimage* **37**, 90-101, doi:10.1016/j.neuroimage.2007.04.042 (2007).

46 Pruim, R. H. R., Mennes, M., Buitelaar, J. K. & Beckmann, C. F. Evaluation of ICA-AROMA and alternative strategies for motion artifact removal in resting state fMRI. *Neuroimage* **112**, 278-287, doi:10.1016/j.neuroimage.2015.02.063 (2015).

47 Pruim, R. H. R. *et al.* ICA-AROMA: A robust ICA-based strategy for removing motion artifacts from fMRI data. *Neuroimage* **112**, 267-277, doi:10.1016/j.neuroimage.2015.02.064 (2015).

48 Jenkinson, M. & Smith, S. A global optimisation method for robust affine registration of brain images. *Med Image Anal* **5**, 143-156, doi: 10.1016/S1361-8415(01)00036-6 (2001).

49 Serag, A. *et al.* Construction of a consistent high-definition spatio-temporal atlas of the developing brain using adaptive kernel regression. *Neuroimage* **59**, 2255-2265, doi: 10.1016/j.neuroimage.2011.09.062 (2012).

50 Avants, B. B. *et al.* A reproducible evaluation of ANTs similarity metric performance in brain image registration. *Neuroimage* **54**, 2033-2044, doi:10.1016/j.neuroimage.2010.09.025 (2011).

51 Smith, S. M. *et al.* Advances in functional and structural MR image analysis and implementation as FSL. *Neuroimage* **23**, S208-S219, 10.1016/j.neuroimage.2004.07.051 (2004).

52 Ward, J. H. Hierarchical Grouping to Optimize an Objective Function. *Journal of the American Statistical Association* **58**, 236-244, doi:10.1080/01621459.1963.10500845 (1963).